J. Fluid Mech. (2009), *vol.* 627, *pp.* 379–401.
doi:10.1017/S0022112009005941 Printed in the United Kingdom

Directional locking and deterministic separation in periodic arrays

JOELLE FRECHETTE AND GERMAN DRAZER†

Chemical & Biomolecular Engineering Department, Johns Hopkins University, Baltimore, MD 21218, USA

(Received 7 April 2008 and in revised form 8 January 2009)

We investigate the dynamics of a non-Brownian sphere suspended in a quiescent fluid and moving through a periodic array of solid obstacles under the action of a constant external force by means of Stokesian dynamics simulations. We show that in the presence of non-hydrodynamic, short-range interactions between the solid obstacles and the suspended sphere, the moving particle becomes locked into periodic trajectories with an average orientation that coincides with one of the lattice directions and is, in general, different from the direction of the driving force. The locking angle depends on the details of the non-hydrodynamic interactions and could lead to vector separation of different species for certain orientations of the external force. We explicitly show the presence of separation for a mixture of suspended particles with different roughness, moving through a square lattice of spherical obstacles. We also present a dilute model based on the two-particle mobility and resistance functions for the collision between spheres of different sizes. This simple model predicts the separation of particles of different size and also suggests that microdevices that maximize the differences in interaction area between the different particles and the solid obstacles would be more sensitive for size separation based on non-hydrodynamic interactions.

1. Introduction

The transport of suspended particles through porous media is central to a wide range of separation techniques that rely on the principle that the trajectories followed by the suspended species depend on their interaction with the porous material. In many cases, it is the geometrical structure of the stationary phase that is the main factor influencing the transport of suspended species in the mobile phase. These geometric (or confinement) effects are most important when the pore dimensions are of the same order as those of the transported species. Two clear examples of separation approaches based on geometric effects are size-exclusion chromatography and hydrodynamic chromatography. In both cases the separation is driven by the degree of hindrance on the transport of finite-size particles caused by the porous structure (Giddings 1991). Therefore, controlling the structure of the stationary phase is an important aspect in the development of an effective separation media. The advent of microfabrication techniques, and more specifically that of soft lithography, has led to the design of microfluidic devices with features in the micron and sub-micron scales. This has allowed for the successful miniaturization of various separation techniques,

† Email address for correspondence: drazer@jhu.edu

including those based on steric and hydrodynamic effects (Slater *et al.* 2000; Blom *et al.* 2003; Khandurina & Guttman 2003; Tegenfeldt *et al.* 2004; Vilkner, Janasek & Manz 2004; Li, Huang & Chang 2005; Szekely & Guttman 2005; Dittrich, Tachikawa & Manz 2006; Szatai & Guttman 2006; Pamme 2007).

The ability to fine-tune the geometry and chemistry of the pore space at scales comparable to the size of the transported particles opens the door to the development of novel separation methods that go beyond the miniaturization of traditional techniques (Duke 1998; Squires & Quake 2005; Eijkel & van den Berg 2006). In traditional separation columns, the random nature of the pore space means that the separative displacement of different species is the average behaviour of an inherently stochastic process. In fact, traditional theories focus on the average transport properties of these systems, such as the average velocity of suspended particles and the hydrodynamic dispersion resulting from the disordered structure of the pore space (Bear 1988; Giddings 1991). This is in sharp contrast with recent microdevices that use ordered arrays of solid obstacles to induce particle separation by deterministic lateral displacements. This approach is based on to a transport regime that is not accessible with a random porous material – and their associated theories (Huang *et al.* 2004; Davis *et al.* 2006; Inglis *et al.* 2006). Although the exact mechanism causing deterministic separation is not fully understood (a phenomenological model is discussed in Inglis *et al.* 2006) it is clear that the hydrodynamic interaction of the suspended particles with the array of obstacles plays an important role. It is thus important to investigate the trajectories followed by individual particles as they move through an ordered pattern of solid obstacles. In particular, studies in the regime of high Pe number would truly explore the deterministic behaviour and would showcase the physics causing the observed separation. A better understanding of the motion of individual particles would allow for the design of periodic microstructures that optimize the separation of a given mixture of suspended species.

In this work, we describe the dynamics of a non-Brownian sphere suspended in a quiescent fluid and moving through a periodic array of solid obstacles under the action of a constant external force. We show that particles become locked into periodic trajectories with an average orientation that coincides with one of the lattice directions (directional/phase locking). Phase-locking behaviour is common to transport through periodic structures in other systems, such as the motion of vortices through periodic pinning potentials in superconductors (Marconi *et al.* 2000), the transport of colloidal particles through optical tweezer arrays (Grier 2003) and others (Korda Taylor & Grier 2002; Reichhardt & Reichhardt 2004; Lacasta *et al.* 2006). In the case studied here, we show that this macroscopic behaviour is caused by non-hydrodynamic, short-range interactions between the suspended spheres and the solid obstacles. Such short-range interactions can originate, for example, from the (unavoidable) deviations from the idealization of perfectly smooth spheres when considering particle–obstacle hydrodynamic interactions. Indeed, our results show that a periodic microstructure could induce separation based on the degree of surface roughness of the spherical particles.

Our work explores the deterministic motion of particles, a different regime than that investigated in the pioneering work of Brenner (1980) and Brenner & Adler (1982), which provided the general framework of macrotransport theory to analyse the motion of Brownian particles in spatially periodic microdevices (see also Brenner & Edwards 1993). Macrotransport theory can be used to describe transport under the action of the driving fields commonly employed in separation sciences, i.e. external forces such as gravity or electric fields and pressure-driven flows. Analogous theoretical

tools have been developed in the context of stochastic processes to solve the Fokker–Planck equation in periodic systems (Risken 1989; Reimann 2002). Dorfman & Brenner (2001) first analysed the behaviour of micropatterned devices in the context of macrotransport theory, and termed these techniques *vector chromatography*. In vector chromatography different species migrate at different angles with respect to the underlying lattice of the periodic pattern of obstacles, which could lead to the development of continuous flow separations (Pamme 2007). Dorfman & Brenner (2001) analysed in detail the transport of suspended particles through a sequence of fluid layers of different viscosity and showed that a uniform external force can induce concentration gradients and diffusive fluxes that lead to migration angles which depend on the Péclet number of the different species. Similar results were obtained for transport in periodic potential fields (see the early work by Nitsche & Brenner 1988 and more recent references in the review by Eijkel & van den Berg 2006). Analogous results were also obtained in the case of patterns of solid obstacles but only for tracer particles with spatially uniform mobilities (see the original work by Ertas 1998 and Duke & Austin 1998 and a more detailed analysis by Keller, Marquardt & Bruder 2002). Recent work, however, shows that finite-size effects are crucial to the observed separation in microdevices (Austin *et al.* 2002; Cabodi *et al.* 2002; Dorfman & Brenner 2002; Huang *et al.* 2002; Tegenfeldt *et al.* 2004; Li & Drazer 2007). Phillips, Deen & Brady (1989, 1990) studied the convective motion of finite-size spherical particles through periodic arrays of bead-and-string fibres aligned perpendicular to the flow. However, they were interested in the behaviour at low Péclet (*Pe*) numbers and did not investigate the trajectories of individual particles in the deterministic limit.

Here, we investigate the case of finite-size particles in the limit of high Péclet numbers (which corresponds to the deterministic transport of non-Brownian particles) in the presence of particle–obstacle hydrodynamic interactions. Specifically, we will show that the presence of directional locking can induce size-based separation of particles by *deterministic lateral displacement*.

2. Model system and simulation methods

Ordered arrays of cylinders, and other spatially periodic systems, have been extensively used to investigate transport phenomena in porous media. In these models of porous media it is possible to calculate pure-fluid average transport properties, such as the macroscopic permeability of the system in different directions (Hasimoto 1959). In addition, the description of solute (tracer) transport in these model systems reduces to a convection–diffusion problem in a single unit cell with periodic boundary conditions. Macroscopic parameters such as the asymptotic hydrodynamic dispersion can then be calculated using macrotransport theory (Brenner 1980; Koch *et al.* 1989; Edwards *et al.* 1991). The transport of finite-size particles through spatially periodic porous media constructed by ordered (and disordered) arrays of cylinders have also been investigated in previous studies, mostly in the context of filtration theory. However, these studies focused on the case of a large aspect ratio between the transported particles and the cylinders (collectors) and either neglected hydrodynamic interactions or approximated them by the hydrodynamic forces between a spherical particle and a flat wall (Masliyah & Bhattacharjee 2006). In addition, there is no analytical expression available for the resistance tensor for an arbitrary sphere–cylinder configuration. Therefore, we follow the approach by Phillips *et al.* (1989) and consider a simpler model, which still captures the structure of the real system

but for which we can calculate the two-particle (PP) sphere–obstacle hydrodynamic interaction. That is we consider a solid, non-Brownian spherical particle of radius a_1 suspended in a Newtonian fluid and driven through a spatially periodic configuration of $N-1$ fixed spheres of radius a_2 by a constant external force. Although here we do not consider motion in the direction of the cylinder axes, an analogous model that could incorporate such motion would consist of bead-and-string fibres aligned perpendicular to the flow (Phillips *et al.* 1989, 1990). Let us note that, in spite of the simple nature of this model, it has been shown to capture the behaviour of several transport properties of real systems, including the permeability perpendicular to and along the cylinders, as well as the hindered diffusivity of the suspended particles as a function of the volume fraction or porosity of the media (Phillips *et al.* 1989). In addition, experimentally measured PP sphere–cylinder interactions have been shown to be similar to sphere–sphere interactions over a wide range of separations (Adamczyk, Adamczyk & Vandeven 1983).

In the limit of low Reynolds numbers, the velocities of the spheres are a linear transformation of the hydrodynamic forces acting on them:

$$\boldsymbol{F} = \boldsymbol{R} \cdot \boldsymbol{u}, \tag{2.1a}$$

$$\boldsymbol{u} = \boldsymbol{M} \cdot \boldsymbol{F}, \tag{2.1b}$$

where $\boldsymbol{R}$ is the resistance matrix; $\boldsymbol{M}$ is the mobility matrix; $\boldsymbol{u}$ is the $6N$ vector with all the linear and angular velocity components; and $\boldsymbol{F}$ is the $6N$ vector of hydrodynamic forces and torques acting on the spheres. In addition, in the absence of inertia, the total force on each particle is zero. Then, if the mobile sphere is *particle 1* and if the remaining $N-1$ spheres are fixed, we obtain the following system of equations (Morris & Brady 1998):

$$\begin{pmatrix} 0 \\ \boldsymbol{F}' \end{pmatrix} = \boldsymbol{R} \cdot \begin{pmatrix} \boldsymbol{u}_1 \\ 0 \end{pmatrix} + \begin{pmatrix} \boldsymbol{F}^p \\ 0 \end{pmatrix}, \tag{2.2}$$

where $\boldsymbol{F}^p$ is the external force acting on the moving sphere and $\boldsymbol{F}'$ corresponds to the forces and torques necessary to keep the other $N-1$ particles fixed. Both $\boldsymbol{R}$ and $\boldsymbol{M}$ depend only on the spatial configuration of the particles, and their numerical calculation is described in § 2.1 and § 2.2. Once the mobility or resistance matrix is determined for a given configuration of the spheres, we can obtain the velocity of the moving particle, $\boldsymbol{u}_1$, from (2.2). We then calculate the position of the moving sphere a short time later and repeat the procedure to generate its trajectory.

2.1. *Stokesian dynamics*

We use the Stokesian dynamics (SD) method to calculate the hydrodynamic interactions in the case of monodisperse spheres ($a = a_1 = a_2$). Briefly, SD combines a far-field multipole expansion for the grand mobility matrix (neglecting terms higher than quadrupoles) with a pairwise additive calculation of the lubrication forces (see Durlofsky, Brady & Bossis 1987 and Brady & Bossis 1988 for a detailed description of the SD method). The grand mobility matrix is inverted at every time step to calculate the velocity of the moving particle. A short-ranged, repulsive force is usually introduced between the spheres to qualitatively model non-hydrodynamic effects such as surface roughness. This repulsive force also prevents the overlap between spheres when using a constant time step in the trajectory integration. In this work we use the following expression for the repulsive interparticle force, already well-tested in the

context of SD:

$$\boldsymbol{F}_{\alpha\beta} = \frac{F}{r_c}\frac{\mathrm{e}^{-\xi/r_c}}{1-\mathrm{e}^{-\xi/r_c}}\boldsymbol{e}_{\alpha\beta}\,, \tag{2.3}$$

where $\boldsymbol{F}_{\alpha\beta}$ is the force exerted on sphere α by sphere β; F is a parameter that determines the magnitude of this force; r_c is the characteristic range of the force; ξ is the separation between the surfaces of the two spheres divided by a; and $\boldsymbol{e}_{\alpha\beta}$ is the unit vector connecting their centres pointing from β to α. In what follows all the variables are made dimensionless with the average particle size $a = (a_1 + a_2)/2$ as the characteristic length and a/U_S as the characteristic time, where $U_S = F^p/6\pi\mu a$ is the Stokes velocity in an unbounded fluid. The non-hydrodynamic interparticle force have a cutoff distance ϵ such that repulsive interactions are present only for $\xi < \epsilon$. For a typical simulation we use $r_c = \epsilon$ and $F = 0.1$. We will see in § 3 that this choice of parameters gives results that are consistent with a hardcore model of surface roughness with relative magnitude ϵ. Finally, we also set the magnitude of the external force acting on the moving sphere to be $|F^p| = F$.

2.2. *Two-particle simulations*

Two-particle (PP) simulations were performed using the mobility functions given by Jeffrey & Onishi (1984). Consider two particles with radii a_1 and a_2 separated by a distance r. Let us define the size ratio $\lambda = a_2/a_1$, the non-dimensional separation $s = 2r/(a_1 + a_2) = r/a$ and the non-dimensional gap between the particles $\xi = s - 2$. Following the notation of Jeffrey & Onishi (1984), all the components of the mobility matrix are written in terms of scalar functions $x^P_{\alpha\beta}$ and $y^P_{\alpha\beta}$, where α and β are either particle 1 or particle 2 and P is one of the tensors ($\boldsymbol{A}$, $\boldsymbol{B}$ or $\boldsymbol{C}$) in the mobility matrix that relates the forces on particle α with the velocity of particle β. Expressions for these scalar functions are given in the far-field approximation, $s \gg 2$, and in the lubrication approximation, $\xi \ll 1$. In our simulations, we use the far-field expressions, with errors in the multipole expansion of the scalar functions $O(1/r^{11})$ or smaller, for $s \geqslant s_c = 2.05$, and the lubrication approximation, for $s < s_c = 2.05$. We shall show that for two equal spheres this choice of s_c gives reasonable agreement with the solutions obtained by SD simulations. The equations of motion are integrated using a small time step Δt in the range 10^{-3}–10^{-5} depending on the minimum separation ξ_{min} between the spheres during the encounter.

3. Hydrodynamic interactions and two-particle trajectories

During the motion of a freely suspended sphere past a fixed one, lubrication forces prevent the two particles from touching, but the two spheres could become arbitrarily close to each other during the encounter. It is likely then that small deviations from the mathematical idealization of perfectly smooth spherical particles, e.g. the presence of surface roughness, would have an effect on the particle trajectories whenever the minimum separation during a collision becomes comparable to the surface roughness. In the analogous case of sheared suspensions, for example, it has been argued in both experimental and numerical studies that the presence of nearly touching collisions leads to measurable macroscopic effects induced by short-range, non-hydrodynamic forces between particles (Gadala-Maria & Acrivos 1980; daCunha & Hinch 1996; Rampall, Smart & Leighton 1997; Drazer *et al.* 2002*b*, 2004; Davis *et al.* 2003). It is important then to investigate the effect that PP collisions have on the macroscopic trajectory of the spheres in the presence of non-hydrodynamic forces.

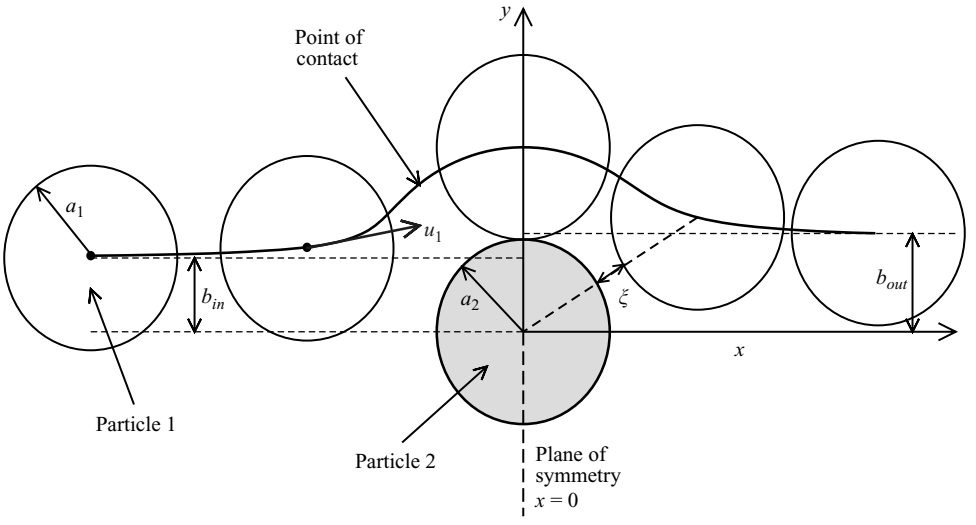

FIGURE 1. Schematic view of the trajectory resulting from the collision of a freely suspended sphere (particle 1), on which a constant external force is applied, with a sphere that remains fixed at the centre (particle 2).

We consider planar collisions, in which an incoming sphere (particle 1) moves under the action of a constant external force, $\boldsymbol{F} = F\mathbf{e}_x$, towards a fixed sphere at the origin (particle 2), as shown in figure 1. The incoming (outgoing) 'collision parameter' b_{in} (b_{out}) is defined as the perpendicular distance between the centre of the fixed sphere and the velocity of the incoming (outgoing) particle (Goldstein 1980). The linearity and reversibility of the equations of motion at zero Reynolds number require that the trajectory resulting from the collision between two perfectly smooth spheres be symmetric about the plane perpendicular to the driving force that contains the centre of the fixed particle (Ekiel-Jezewska *et al.* 1999). In addition, lubrication forces prevent the particles from touching, independent of the value of the collision parameter b_{in} (Jeffrey & Onishi 1984). On the other hand, the minimum surface separation between the two spheres during a collision, ξ_{min}, becomes arbitrarily small for $b_{in} \to 0$. Then, for a given magnitude of the surface roughness, ϵ, we can define a critical collision parameter, $b_c(\epsilon)$, such that for $b_{in} < b_c$ the minimum separation on a purely hydrodynamic trajectory is smaller than the roughness of the particle, $\xi_{min} < \epsilon$, and the non-hydrodynamic effects are expected to significantly alter the collision trajectory. Note that $b_c(\epsilon)$ is simply the inverse function of $\xi_{min}(b_{in})$.

The dependence of the minimum separation, ξ_{min}, on the collision parameter, b_{in}, is obtained from collision trajectories calculated in the case in which only hydrodynamic interactions are present. The trajectories are computed using either SD or PP simulations without repulsive forces and significantly reducing the time step to prevent overlap between the particles.

The simulations show that the minimum separation between the particles becomes extremely small, decreasing by six orders of magnitude to $\xi_{min} \sim 10^{-6}$, for collision parameters ranging from $b_{in} = 2$ to $b_{in} = 0.65$ (see figure 2). Let us note that it is meaningless to consider even smaller separations. First of all, the typical roughness observed in rheological experiments with solid particles was found to be $\epsilon \sim 10^{-3}$–10^{-2} (Smart & Leighton 1989). In addition, the microfluidic systems discussed in the introduction are intended to separate particles smaller than 100 μm. Therefore, a

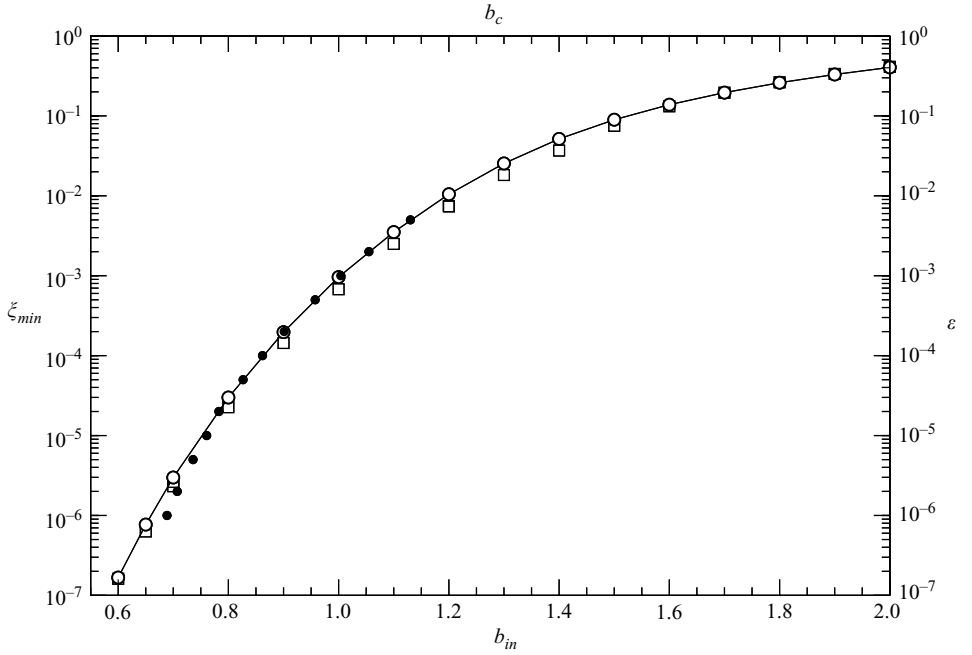

FIGURE 2. Minimum separation during purely hydrodynamic collisions, ξ_{min}, as a function of the impact parameter, b_{in}. The same curve can be used to obtain the critical collision parameter, b_c, as a function of the relative magnitude of the surface roughness, ϵ. Open circles correspond to SD. Open squares correspond to PP simulations. Solid circles correspond to the outgoing collision parameter, b_{out}, as a function of the roughness magnitude, ϵ, obtained using SD simulations with non-hydrodynamic interactions ($b_{in} = 0.1$; see discussion in the text).

minimum separation $\xi_{min} \sim 10^{-5}$ corresponds to a suspended particle coming within atomic distance from the surface of a fixed sphere. For such small separations the spheres cannot be considered to be perfectly smooth. Moreover, corrections to the continuum approximation become important at these small separations (Drazer *et al.* 2002*a*, 2005*a*,*b*).

The fact that a wide range of collision parameters would lead to minimum separations between particles that are extremely small, e.g. $\xi_{min} < 10^{-4}$ for $0 < b_{in} \lesssim 0.9$, implies that the particle trajectory should be affected readily by non-hydrodynamic interactions caused by, for example, surface roughness. We investigate the non-hydrodynamic effects on the trajectory of a moving particle by performing two sets of SD simulations in the presence of the repulsive force given by (2.3). In one case, we fix the magnitude and range of the non-hydrodynamic force ($F = 0.1$; $\epsilon = 10^{-3}$) and study the trajectories resulting from different collision parameters. In the second case, we arbitrarily fix the collision parameter to $b_{in} = 0.1$ and study collision trajectories for different values of the relative roughness of the particles.

In the first case, trajectories are symmetric for collision parameters larger than a critical value $b_c \approx 1$ (see figure 3). Trajectories corresponding to $b_{in} < b_c$ are asymmetric and collapse into a single outgoing trajectory with $b_{out} \approx b_c$. This irreversible collapse into a single trajectory has a major impact in the trajectory of the particles through an array of obstacles, creating periodic trajectories that act as attractors for any initial position of the moving particle, a behaviour discussed in detail in the next section.

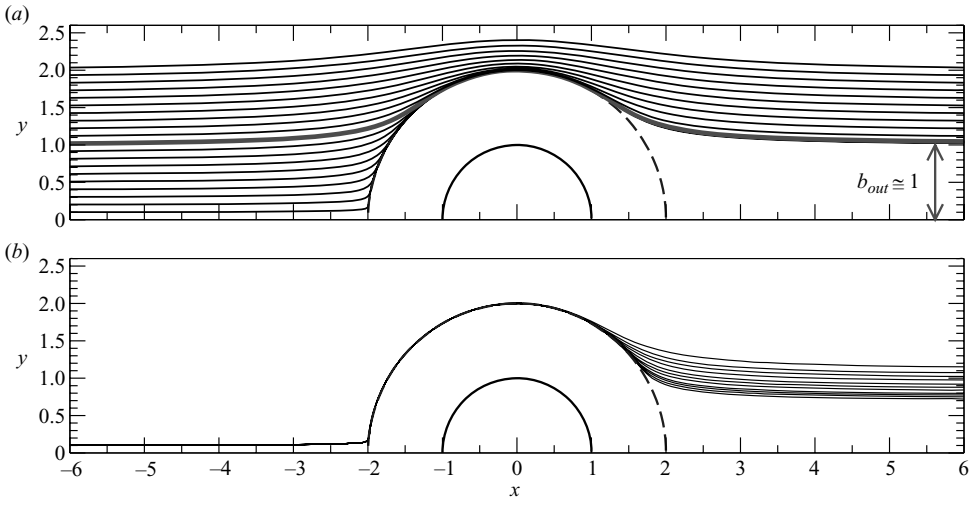

FIGURE 3. Collision trajectories calculated using SD simulations with non-hydrodynamic interactions. (*a*) Trajectories with varying incoming collision parameter ranging from $b_{in} = 0.1$ to $b_{in} = 2.0$. $\epsilon = 10^{-3}$. (*b*) Trajectories for varying relative surface roughness ranging from $\epsilon = 10^{-1}$ to $\epsilon = 10^{-6}$; $b_{in} = 0.1$.

In the second case, in which we systematically reduce the range of the interparticle force from $\epsilon = 10^{-1}$ to $\epsilon = 10^{-6}$, the trajectories become more symmetric as the roughness becomes smaller. Analogous trajectories with varying asymmetry depending on the particle roughness have been previously reported for the collision between two spheres in a sheared suspension (daCunha & Hinch 1996). These trajectories for different roughness values are also consistent with an irreversible collapse into a single outgoing trajectory with $b_{out}(\epsilon) \approx b_c(\epsilon)$, as shown in figure 2. The collapse into a single trajectory depends, however, on the interparticle force used to model roughness effects. The non-hydrodynamic interaction used here is similar to a hard-sphere potential, with no interaction for $\xi > \epsilon$ and infinite repulsion for $\xi < \epsilon$ (Allen & Tildesley 1989). Softer interactions, such as the algebraic soft-sphere potentials discussed in Allen & Tildesley (1989), would probably lead to a spread of the outgoing trajectories. However, hard-sphere type of potentials, in which particles cannot approach each other beyond a minimum separation, are probably the simplest approximation of the behaviour of particle–particle contact due to roughness and have been successfully used to investigate roughness effects in suspension flows (Smart & Leighton 1989; Davis 1992; Zeng, Kerns & Davis 1996; Rampall *et al.* 1997; Ekiel-Jezewska *et al.* 1999, 2002; Zhao & Davis 2002, 2003; Davis *et al.* 2003). The effect of an algebraic repulsion on the trajectories is discussed again in the next section.

In summary, for a given particle roughness ϵ, we have two types of collisions: (i) purely hydrodynamic collisions for all $b_{in} > b_c(\epsilon)$, in which case the trajectory is symmetric, and the outgoing streamline is the same as the incoming one, $b_{out} = b_{in}$; and (ii) touching collisions, for all $b_{in} < b_c(\epsilon)$, which result in asymmetric trajectories that collapse into a single outgoing impact parameter, $b_{out} = b_c(\epsilon)$. Therefore, knowing $b_c(\epsilon)$ we can determine the trajectory of any binary collision. It is important to note that a similar behaviour is expected in Stokes flows for an arbitrary driving field that preserves the symmetry of the problem, including electrophoretic fields and pressure-driven flows. In this case, the particle will follow symmetric trajectories in

the absence of non-hydrodynamic interactions, from which the minimum separation, ξ_{min}, as a function of the incoming impact parameter, b_{in}, can be determined. Then, the presence of roughness would result in a critical collision parameter, $b_c(\epsilon)$, equivalent to that in the constant force case. Therefore, collisions with $b_{in} < b_c(\epsilon)$ collapse into a single outgoing trajectory with $b_{out} = b_c(\epsilon)$ and the overall result of a PP collision is completely analogous to the constant force case. The driving field determines, however, the minimum separation corresponding to a given impact parameter and could lead to different scaling relations between b_{in} and ξ_{min}.

The numerical results presented above are in qualitative agreement with the few experiments that investigate the collision between a moving and a fixed sphere. Ekiel-Jezewska *et al.* (1999), for example, report the existence of a critical collision parameter. Malysa *et al.* (1986) studied the motion of a sphere sedimenting past a second sphere attached to a flat wall. They also reported the existence of a critical collision parameter, $b_c^{exp} = 1.34$, below which the trajectories are asymmetric. They also observe a collapse of all the receding trajectories, and in agreement with a hard-sphere type of contact between the spheres, the receding collision parameter for the asymmetric trajectories is $b_{out}^{exp} = 1.3 \approx b_c^{exp} = 1.34$. The experiments used spheres with 3 mm radius and an estimated maximum roughness as large as a few microns, which corresponds to $\epsilon \sim 10^{-3}$. The predicted critical collision parameter in our simulations for $\epsilon \sim 10^{-3}$, that is $b_c \sim 1.1$, is in fair agreement with the experimental value, $b_c^{exp} \approx 1.3$, especially if one takes into account the large sources of uncertainty in the experimental measurements. On the other hand, it is not our intention to accurately model the $b_c(\epsilon)$ curve but to understand the effect that such a steep curve, according to which particle–particle solid contact might be expected for impact parameters as large as $b_c \sim 1$, has on the trajectory of the particles in periodic arrays.

4. Particle trajectories in a periodic array of obstacles

In this section we investigate the effect that irreversible collisions have on the macroscopic trajectory of a non-Brownian sphere moving through a periodic array of obstacles under the action of a constant force. In particular, we are interested in modelling the motion of a non-Brownian particle through an array of cylindrical obstacles and characterizing the relation between the asymptotic angle α of individual trajectories and the orientation of the external force θ. As discussed before, we represent the obstacles by a two-dimensional square lattice of fixed spheres (spheres' radii a_2, lattice parameter l and dimensionless lattice parameter $\ell = l/a_2$). We calculate the two-dimensional trajectories followed by freely suspended spheres of radius a_1 moving in the plane x–y of the fixed spheres under the action of a constant force $\boldsymbol{F}^p = F_x^p \boldsymbol{e}_x + F_y^p \boldsymbol{e}_y$ (see figure 4 for a schematic view of the system).

Let us first analyse the deterministic (high-Péclet-number limit) trajectory followed by a point particle moving through the same array of obstacles. Specifically, consider the streamlines in a pressure-driven (or gravity-driven) flow with average velocity $\boldsymbol{U} = U_x \boldsymbol{e}_x + U_y \boldsymbol{e}_y$. The permeability of the square lattice is isotropic, and therefore, the average velocity is parallel to the direction of the driving force. In general, the study of the flow generated by differential equations on the torus (two-dimensional periodic fields) dates back to Poincaré (Arnold 1988), and recent results for incompressible flows with non-zero average velocity show (i) that the asymptotic slope of the streamlines (also called the *rotation number*) is parallel to $\boldsymbol{U}$ ($\alpha = \theta$) and (ii) that the existence of unbounded periodic trajectories depends on the commensurability of the mean drift (Weinan 1992; Fannjiang & Papanicolaou 1994). Specifically, when

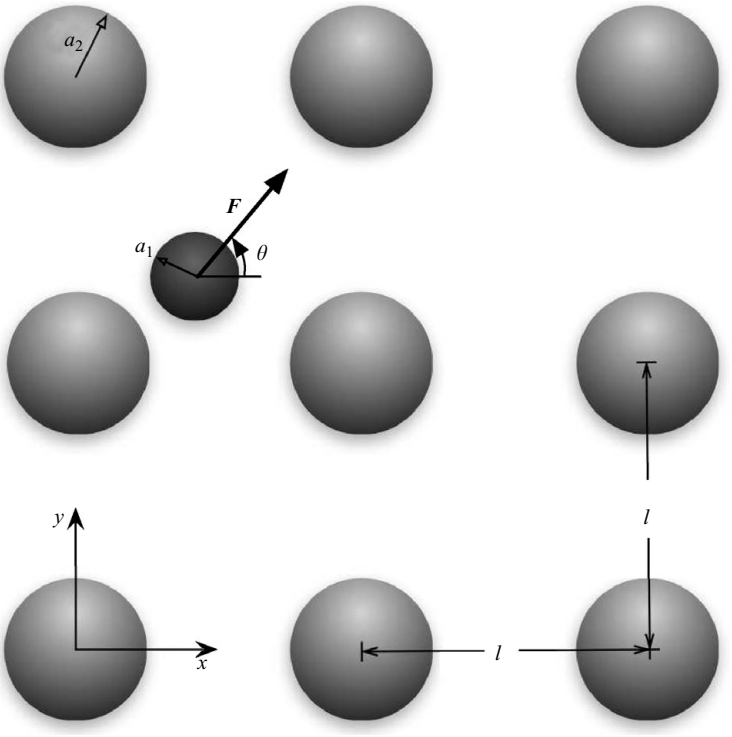

FIGURE 4. Schematic representation of a sphere (*particle 1*; radius a_1) moving in a two-dimensional periodic lattice of $N-1$ spherical particles of radii a_2. The lattice parameter is $l = \ell\, a_2$. A constant force F is applied on *particle 1* at an angle θ with respect to the x-axis.

U_x and U_y are incommensurate, there are no unbounded periodic streamlines, and any unbounded trajectory is ergodic in the region of open streamlines. On the other hand, U_x and U_y are commensurate if and only if there is an unbounded periodic trajectory (Weinan 1992; Fannjiang & Papanicolaou 1994). Similar conclusions were reached by Koch *et al.* (1989).

Some of the discussed properties of two-dimensional streamlines also apply to the trajectories described by finite-size particles, even though the flow field is no longer incompressible in the latter case. First, in the absence of inertia (Stokes regime) two trajectories cannot cross each other, since the velocity of a particle is fully determined by its position. Therefore, all unbounded trajectories have the same asymptotic slope, which can thus be determined from a single simulated trajectory with arbitrary initial conditions. Second, the existence of periodic trajectories can be easily demonstrated in the case in which the external force is oriented in one of the main symmetry directions, that is $\boldsymbol{F}^p = F^p \boldsymbol{e}_x$, $\boldsymbol{F}^p = F^p \boldsymbol{e}_y$ or $F_x^p = F_y^p$. These directions define planes of both translational and reflectional symmetries and together with the symmetry and reversibility of the Stokes equations require that all the trajectories are periodic. Finally, the existence or not of periodic trajectories for an arbitrary orientation of the external force has, to our knowledge, not been determined for purely hydrodynamic interactions. However, we shall see that the presence of non-hydrodynamic forces induces periodic trajectories for both commensurate and incommensurate orientations of the driving force.

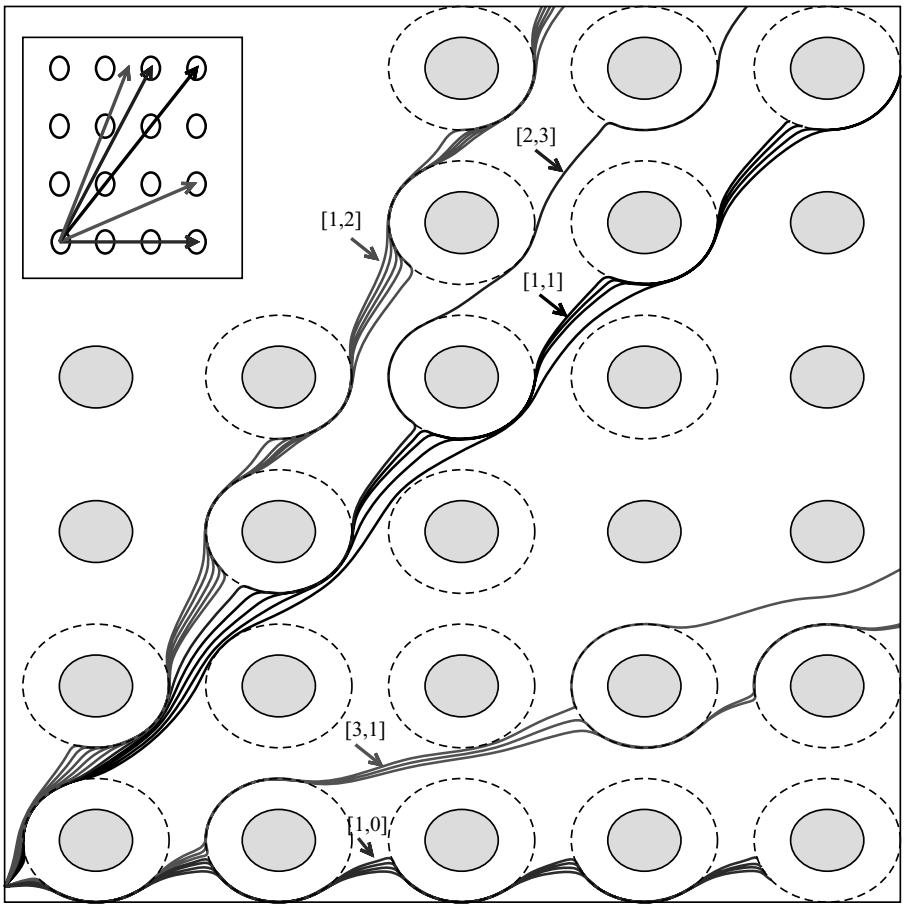

FIGURE 5. Periodic trajectories obtained at different forcing angles θ. The lattice parameter is $\ell = 5$, and the range of the repulsive force is $\epsilon = 10^{-3}$. Trajectories are grouped according to their macroscopic motion. From top to bottom: (i) lattice direction [1,2]; $\alpha = 71.56°$; forcing directions: $\theta = 58.50°, 60.75°, 63.00°, 65.25°, 67.50°$; (ii) lattice direction [2,3]; $\alpha = 56.31°$; forcing direction: $\theta = 56.25°$; (iii) lattice direction [1,1]; $\alpha = 45.00°$; forcing directions: $\theta = 54.00°, 51.75°, 49.50°, 47.25°$; (iv) lattice direction [3,1]; $\alpha = 18.43°$; forcing directions: $\theta = 20.25°, 18.00°, 15.75°$; (v) lattice direction [1,0]; $\alpha = 0°$; forcing directions: $\theta \leqslant 13.50°$. The lattice directions at which directional locking occurs are shown in the inset.

4.1. *Case I: $a = a_1 = a_2$, Stokesian dynamics simulations*

We simulate the trajectories of non-Brownian particles in the case $a = a_1 = a_2$ by means of SD simulations. We observe that, independent of the orientation of the external force, the suspended spheres describe trajectories that are commensurate with the underlying obstacle lattice (see figure 5). That is the average motion of the particles is in one of the lattice directions, $[p, q]$, with p and q integers and $\alpha_{[p,q]} = \arctan(q/p)$. Thus, in general, the particle will move at an angle that is different from that of the external force. We also observe *directional locking*, in that suspended spheres driven at different angles move, on average, in the same lattice direction. In fact, in figure 5 we show that particles forced at more than 15 different angles get locked into only five different orientations, corresponding to lattice directions [1, 2], [2, 3], [1, 1], [3, 1], [1, 0] (see figure 5). For example, trajectories corresponding to forcing angles

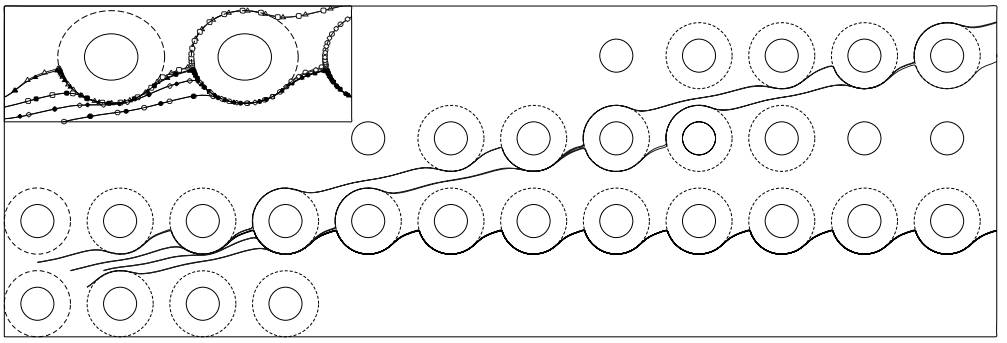

FIGURE 6. Periodic trajectories obtained for different initial conditions and two different relative roughness of the spheres. Lattice parameter $\ell = 5$. For all the trajectories the forcing direction is $\theta = 14.00°$. Top trajectories (open symbols in the inset) correspond to $\epsilon = 10^{-3}$ and move in the lattice direction [4,1], $\alpha = 14.04°$. This corresponds to a small deviation in the direction of motion, that is $\alpha - \theta \approx 0$. Bottom trajectories (closed symbols in the inset) correspond to $\epsilon = 10^{-2}$ and move in the [1,0] lattice direction, $\alpha = 0°$, corresponding to a large migration angle with respect to the direction of the driving force.

$\theta = 58.50°$, $60.75°$, $63.00°$, $65.25°$ and $67.50°$ move at a macroscopic angle $\alpha = 71.56°$ (lattice direction [1, 2]). The observed directional locking is induced by the presence of non-hydrodynamic forces. We observe that all the trajectories become periodic after a small number of touching collisions, which can be easily explained based on the results obtained for PP collisions. When a moving particle reaches a distance ϵ or smaller from one of the fixed particles, the receding part of the trajectory is analogous to the outgoing trajectory in a touching collision, with $b_{out} = b_c(\epsilon)$. That is for a touching collision the outgoing trajectory is independent of the initial condition. Therefore, a set of incoming trajectories collapses into a single outgoing trajectory, analogous to the case $0 < b_{in} < b_c(\epsilon)$ in the PP case. As a consequence, the next touching collision will lead to the same outgoing trajectory, and the motion becomes periodic thereafter. In fact, in the simple square lattice shown in figure 5 there might be a maximum of two touching collisions in a single period of the trajectory, one with clockwise motion of the centre of the moving sphere during the collision and one with counterclockwise motion. These two touching collisions correspond to positive and negative collision parameters in the PP case. In more complex arrays of obstacles, such as the lattice shown in figure 7, the number of touching collisions in a single period of the trajectory could be as large as $2n$, where n is the number of obstacles in a unit cell. In general, the trajectory repeats itself after the moving sphere comes into contact for a second time with a fixed sphere occupying a specific position in the unit cell.

The fact that the periodic motion of the particles is induced by the non-hydrodynamic forces suggests that different short-range particle–obstacle interactions could lead to vector separation. In fact, the presence of vector separation for equal spheres with different magnitude of the surface roughness is shown in figure 6. Although all the trajectories correspond to an external force with $\theta = 14°$, the motion of the particles is either at $\alpha = 0°$ for $\epsilon = 10^{-3}$ or at $\alpha = 14.04°$, corresponding to the lattice direction [4,1], for smoother spheres with $\epsilon = 10^{-4}$. Note that this is consistent with smoother spheres having smaller migration angles, in this case $\alpha - \theta \approx 0.04$. Particle trajectories do not cross each other, and therefore, the macroscopic direction of motion, α, is independent of the initial position of the particle inside the unit cell.

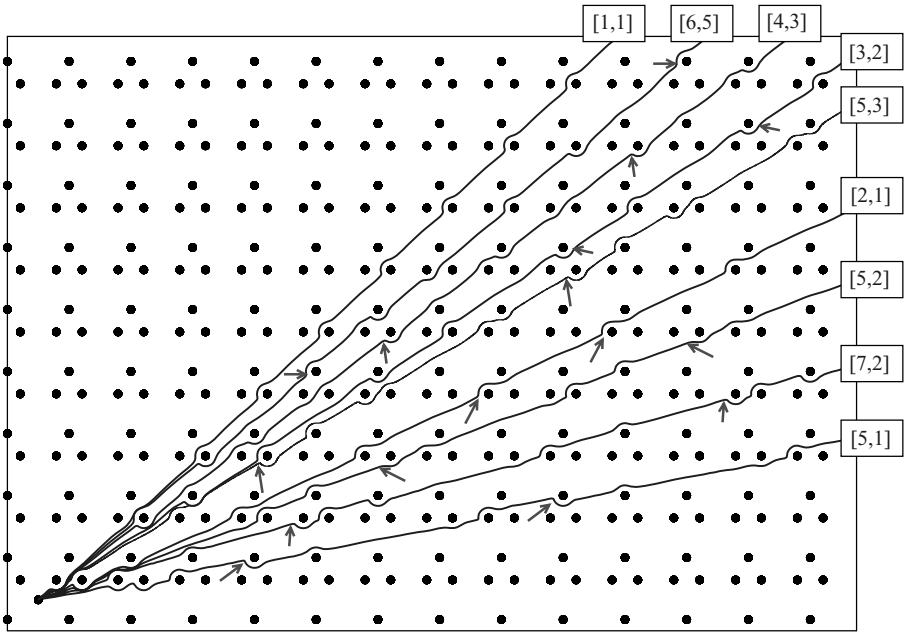

FIGURE 7. Periodic trajectories in a square lattice, $\ell = 12$, with three particles in each unit cell. The position of the obstacles are $(0, \sqrt{3}d/4); (-d/2, -\sqrt{3}d/4); (+d/2, -\sqrt{3}d/4)$ from the centre of the unit cell, forming an equilateral triangle with side $d = 5$. The trajectories correspond to forcing angles (from top to bottom): $\theta = 42.75°, 40.50°, 38.25°, 33.75°, 31.50°, 24.75°, 20, 25°, 15.75°, 11.25°$. The locking directions are indicated in the figure. The beginning and end of a single period in each trajectory are indicated with arrows. The roughness parameter in the SD simulations is $\epsilon = 10^{-3}$.

This is shown in figure 6 and validates the use of individual trajectories to characterize the α versus θ relation.

A periodic motion set by successive touching collisions requires a macroscopic angle of the trajectories that is a commensurate direction of the obstacle lattice. Let us note that, in the obstacle array studied above, the positions of the obstacles coincides with the vertices of the unit cell. In general, a periodic array of obstacles is defined by a Bravais lattice and an arbitrary distribution of obstacles inside the unit cell, i.e. a *basis*. The possible locking directions are given by the symmetry of the Bravais lattice independent of the position of the obstacles inside the unit cell. This is borne out in figure 7, where it is clear that, although the position of the obstacles within the square lattice is different from the previous case, with three obstacles in each unit cell and broken rotational symmetry, the locking angles are, as before, commensurate directions of the square lattice. In figure 7 we explicitly show the periodicity of the trajectories after colliding for a second time with equivalent fixed spheres and the corresponding lattice direction, for several locking angles.

The previous results show that, although the medium permeability is isotropic for a simple fluid, the average motion of finite-size particles is not necessarily in the same direction as the external force, due to the non-hydrodynamic interactions of the suspended particle with the solid obstacles. In addition, the fact that we observe that a finite range of forcing angles leads to the same macroscopic orientation of the particle trajectory implies that even for some commensurate forcing directions

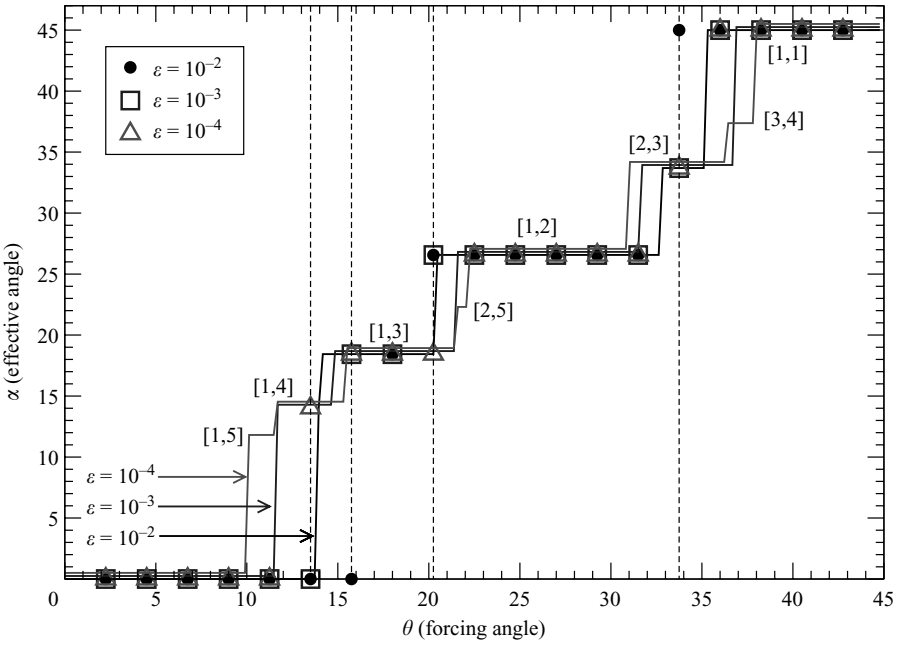

FIGURE 8. Macroscopic orientation of the particle trajectories as a function of the orientation of the driving force, i.e. α versus θ. The lattice is shown in figure 5. The simulations are performed for different surface roughness: closed circles correspond to $\epsilon = 10^{-2}$; open squares correspond to $\epsilon = 10^{-3}$; open triangles correspond to $\epsilon = 10^{-4}$. Solid lines correspond to results obtained in the dilute approximation (see § 4.2). Solid lines are shifted vertically for the sake of clarity.

the particles move at a different angle ($\theta = \arctan(q/p)$ is a dense subset of all the possible angles).

In figure 8 we present the asymptotic angle of motion as a function of the forcing direction for three different magnitudes of the particle roughness. Let us note, first, the Devil's staircase type of structure of this curve, which is typical of phase-locking systems (Bak 1986; Gopinathan & Grier 2004). More importantly, it is clear that there are some forcing angles for which not all the particles move together. That is the macroscopic orientation of the trajectories depends on the roughness of the particles, as previously shown in figure 6. This result indicates that a strategy for vector separation could be based on the details of the particle–obstacle interactions in periodic systems.

Finally, in order to check the generality of the observed locking dynamics, we simulated the trajectory of a particle for different short-range forces, including different magnitudes of the repulsive force given by (2.3) and different magnitudes of a *soft* repulsion term, given by $F_s = A/\xi^2$. Specifically, we first simulated a case similar to those shown in figure 5 with $F = 0.1$, $r_c = 10^{-3}$ and $\epsilon = 10^{-3}$. We then simulated the motion for different magnitudes of the force $F = 1$, 10, 50 and 100. (We also increased the roughness, $\epsilon = 0.01$, and the cutoff radius, $r_c = 0.1$.) Finally, we simulated the case of the soft repulsion force given above for $A = 0.1$, 0.01 and 0.001. In figure 9 we can see that the same locking dynamics are observed in all cases, with the only difference being in the effective migration angle which depends on the non-hydrodynamic force, as shown before.

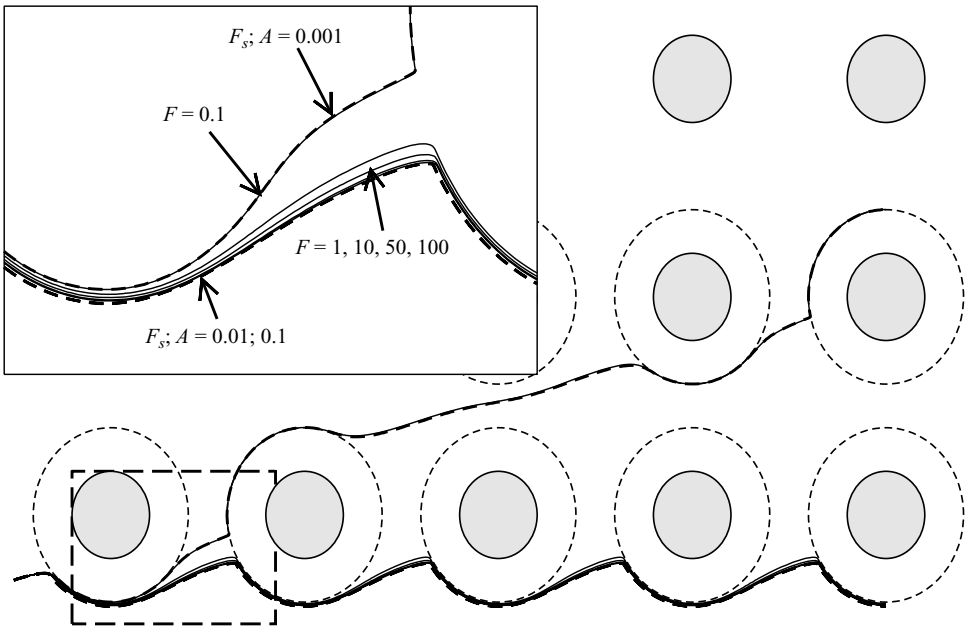

FIGURE 9. Comparison of trajectories obtained using SD simulations for different non-hydrodynamic repulsive forces between the spheres. The different simulations correspond to (i) force given by (2.3) with $\epsilon = 10^{-3}$, $r_c = 10^{-3}$, $F = 0.1$ (solid line); (ii) force given by (2.3) with $\epsilon = 10^{-2}$, $r_c = 0.1$, $F = 1$, 10, 50 and 100 (dashed lines); and (iii) a *soft* repulsive force given by $F_s = A/\xi^2$, with $A = 0.1$, 0.01 and 0.001 (solid lines).

4.2. *Case II: $a_1 \neq a_2$, two-particle collision model*

In the previous section we showed that non-hydrodynamic interactions can lead to vector separation due to a directional locking of the trajectories that depends on the particle roughness. Here, we extend our analysis to particles whose sizes are different from that of the obstacles.

In § 3 we analysed the collision of a moving sphere with a fixed one and showed that, in the presence of non-hydrodynamic forces, there are two types of collisions: collisions leading to symmetric trajectories for $b_{in} > b_c(\epsilon)$ and collisions that collapse into a single receding trajectory with $b_{out} = b_c(\epsilon)$ for $b_{in} \leqslant b_c(\epsilon)$. In the dilute limit, that is for $\ell \gg 1$, we can approximate the particle trajectories by a series of PP collisions joined by motion in straight lines between collisions. In this approximation, the symmetric collisions are irrelevant, in that they do not alter the trajectory of the moving particle. On the other hand, the only effect of the touching collisions is a displacement perpendicular to the direction of motion by $b_{in} - b_{out} = b_{in} - b_c(\epsilon)$.

First, we show in figure 10 that the trajectories obtained using this approximation for the case of equal spheres exhibit, in general, the same macroscopic angle as those calculated from SD simulations. In addition, in figure 8 we compare the α versus θ curve obtained with the present model with the SD results discussed before. Although the transition angles between consecutive plateaus might be slightly different in some cases, the agreement is generally good for all the magnitudes of the particle roughness.

We then use this dilute approximation to investigate directional locking and vector separation in the case of unequal spheres. First, we compute the $b_c(\epsilon)$ curve for different particle sizes, that is $b_c \equiv b_c(\epsilon, \lambda)$. Then, using the dilute approximation we determine the corresponding locking curve $\alpha \equiv \alpha(\theta, \epsilon, \lambda)$. In figure 11($a$) we present

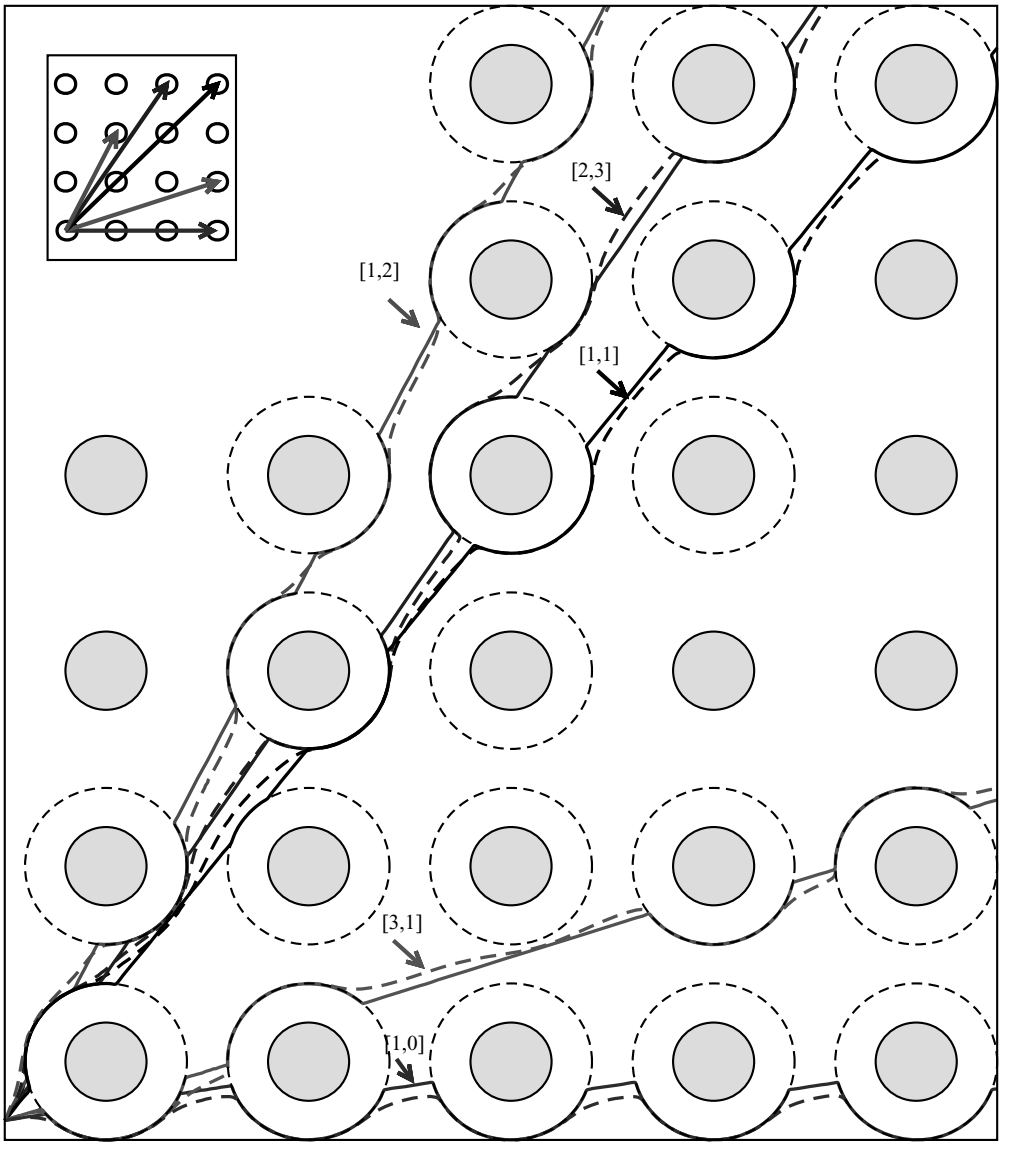

FIGURE 10. Comparison of trajectories obtained in the dilute approximation (§4.2) with those obtained using SD simulations. We compare one trajectory for each of the locking directions presented in figure 5. Solid lines correspond to the dilute approximation. Dashed lines correspond to SD simulations. The locking directions are indicated in the figure.

the minimum separation during collision as a function of the impact parameter, for different size ratios λ. It can be seen that, for a given incoming collision parameter, the minimum separation decreases as the size ratio deviates from one. In other words, for a given relative roughness ϵ, the critical collision parameter $b_c(\epsilon)$ is larger for larger values of λ or $1/\lambda$. These results indicate that a mixture of suspended spheres of different sizes might separate as they move through an array of obstacles. In figure 11(b) we plot the dimensional critical collision parameter, $\tilde{b}_c = b_c(a_1 + a_2)/2$, for a moving particle of size $a_1 = 1$ and various obstacle sizes, $a_2 = \lambda$. It is clear that,

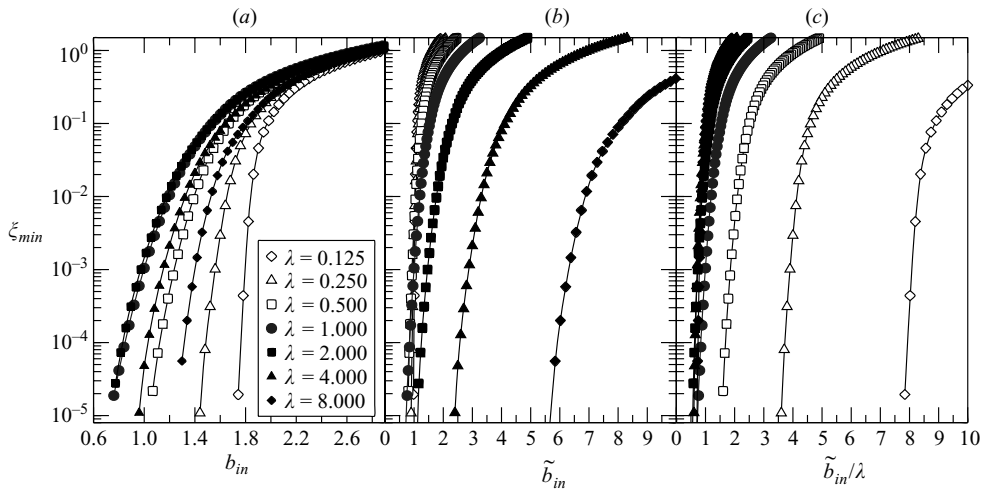

FIGURE 11. Minimum separation during purely hydrodynamic collisions, ξ_{min}, as a function of the impact parameter, for different size ratios, λ. The results correspond to the numerical integration of PP collision trajectories (see § 2.2). The different plots correspond to ξ_{min} as a function of (*a*) the non-dimensional collision parameter b_{in}; (*b*) the collision parameter normalized by the radius of the moving particle $\tilde{b}_{in}$; and (*c*) the collision parameter normalized by the radius of the fixed spheres, $\tilde{b}_{in}/\lambda$.

for a given particle size, obstacles larger than the particle result in larger values of $\tilde{b}_c = b_c(a_1 + a_2)/2$ and the corresponding migration angles (comparing critical collision parameters for a constant roughness). In this dilute approximation, two particles with the same critical collision parameter move at the same macroscopic angle, α, independent of their size. Then, only particles that have different critical collision parameters for a fixed obstacle size, that is $\tilde{b}_c/\lambda$, could potentially separate. To show the possibility for deterministic vector separation based on particle size we analyse in detail the transport of different particles through a square lattice ($\ell = 12$). First, we arbitrarily consider a mixture of particles with the same particle roughness independent of size, that is $\epsilon = 10^{-2}$ for all λ. Then, using the dilute approximation, we calculate the migration angle, $\alpha - \theta$, as a function of the driving direction θ, for different size ratios: $\lambda = 1$, 0.5, 2, 0.25, 4, 0.125, 8. We find the same type of directional locking as in the case of equal size particles (see figure 12). We can also see that the migration angles are larger for particles that are larger than the obstacles ($\lambda < 1$). This is also observed in figure 11(*c*), in which the dimensional critical collision parameter is presented for different sizes of the moving particle and a constant size of the obstacles ($a_2 = 1; a_1 = 1/\lambda$).

Finally, using the migration angles presented in figure 12, we select a driving direction that leads to four different locking angles depending on the size of the particles ($\theta \approx 21^\circ$, see inset in figure 12). We then simulate the transport of a mixture of particles through the square lattice of obstacles. To simulate the motion of all the particles, including the ones that have the same size as the obstacles, we used the dilute approximation. We find the presence of vector separation and observe that, as expected, larger particles ($\lambda < 1$) have larger migration angles (see figure 13). Let us mention that a possible drawback of this separation method is that the migration angle is not necessarily monotonous with particle size, which could make it difficult to separate a mixture with a wide range of particle sizes. Possible solutions to this

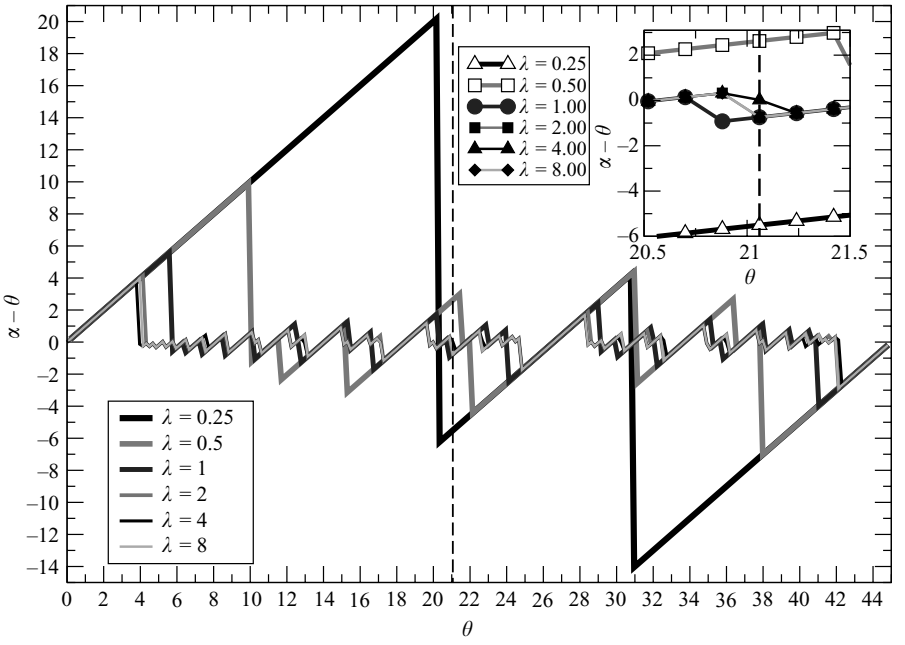

FIGURE 12. Macroscopic migration angle, $\alpha - \theta$, as a function of the orientation of the driving force, θ, for different size ratios, λ. We use a square lattice with $\ell = 12$ to allow for the motion of larger particles. The simulations are performed for a surface roughness $\epsilon = 10^{-2}$. The inset shows in detail the migration angle for a forcing direction $\theta = 21.06^{\circ}$ (corresponding to the dashed vertical line), for which particles migrate at four different directions depending on their size.

problem include (i) using an obstacle pattern in which the orientation relative to the external driving field changes along the device (Huang *et al.* 2004) and (ii) using different obstacle patterns in series. In both cases, one could optimize different parts of the system to separate specific particle sizes.

5. Summary

We investigated the trajectory described by finite-size spherical particles moving through a periodic array of obstacles, using SD simulations as well as PP mobility and resistance functions.

We first considered the collision between a freely suspended particle moving past a fixed one under the action of a constant external force. We characterized the collision trajectories based on the incoming (outgoing) impact parameters, b_{in} (b_{out}). We showed not only that the two spheres could come extremely close to each other during the collision but also that relatively large impact parameters would lead, in principle, to atomic-scale separations for typical particles in microdevices. For example, we estimated that a sphere of radius 100 μm would come within 10Å of the fixed sphere for an impact parameter $\tilde{b}_{in} \approx 75$ μm and a trajectory resulting from purely hydrodynamic interactions. Therefore, even small surface roughness, or other short-range non-hydrodynamic forces, would become important when the particles get sufficiently close, and the trajectory followed by the particles will deviate from the ideal case of two perfectly smooth spheres with purely hydrodynamic interactions calculated in the continuum limit.

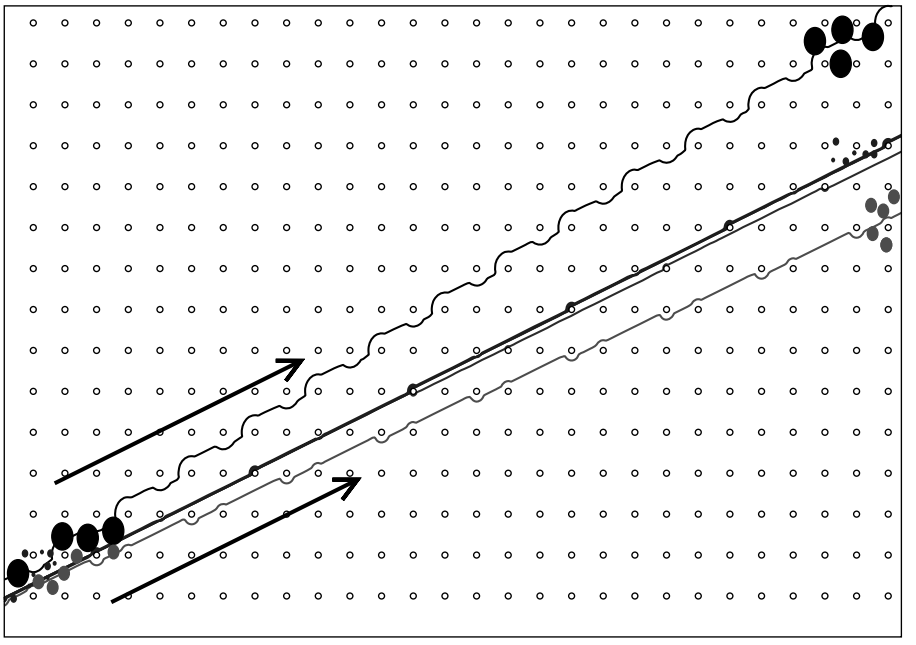

FIGURE 13. Particle trajectories for a mixture of particles of different size in a square lattice with $\ell = 12$ and for the driving angle shown in figure 12, $\theta \approx 21°$. A mixture of particles of different sizes is in fact separated as expected from figure 12. Trajectories are calculated using the dilute approximation discussed in the text.

We then investigated the effect that non-hydrodynamic interactions, such as surface roughness, have on the collision trajectories, by including a short-range repulsive force between the spheres. We showed that if $b_c(\epsilon)$ is the critical impact parameter for which the minimum separation between the spheres becomes equal to the roughness magnitude ϵ, then binary collisions can be divided into two different types: symmetric collisions, due to purely hydrodynamic interactions for $b_{in} > b_c(\epsilon)$, and touching collisions, with $b_{out} \approx b_c(\epsilon)$, for $b_{in} \leqslant b_c(\epsilon)$.

Touching collisions ultimately led to periodic trajectories that acted as asymptotic trajectories (limit cycles) for any initial position of the moving particle. The macroscopic angle of the particles trajectories was always commensurate with the obstacle lattice and exhibited directional locking, in that certain lattice directions lock trajectories over a finite range of force orientations. This results in a Devil's staircase type of curve for the trajectory angle as a function of the angle of the driving force.

The locking angle is determined by the critical collision parameter, which in turn is determined by the non-dimensional magnitude of the surface roughness, ϵ. In fact, we showed that different magnitudes of the surface roughness could lead to different locking angles for certain orientations of the driving force. This result implies that differences in the local, short-range interaction between suspended particles and solid obstacles arranged in a periodic array could lead to vector separation. We explicitly showed the presence of vector separation for a square lattice of obstacles, with particles of equal size migrating at different angles depending on their roughness.

We also compared the SD results with a simple model in which the trajectory of the particles was approximated by a series of PP collisions, connected by straight motion parallel to the external force between collisions (dilute approximation). This simple

model accurately described the dependence of the locking angle on the orientation of the external force for different magnitudes of the relative roughness, even when the non-dimensional distance between obstacles was as small as $\ell = 5$.

Finally, we used this dilute approximation to obtain the particle trajectory for spherical particles of different size. First, we calculated the minimum separation between the spheres during a PP collision as a function of the size ratio λ between the moving sphere and the solid obstacles. We showed that the minimum separation, and therefore the critical collision parameter, depends on the size ratio. This indicates that vector separation could also be based on particle size. In fact, we showed that, for certain force orientations in a simple cubic lattice, particles of different size migrate at different angles. We also showed that, for a given particle size the critical collision parameter is larger for larger obstacles, specially for $\lambda > 1$. On the other hand, for a given obstacle size, the critical collision parameter increases with particle size, specially for $\lambda < 1$. The previous results suggest that microdevices that maximize the difference in interaction area between the different particles and the solid obstacles would be better suited for size separation based on roughness or other non-hydrodynamic repulsive interactions.

The results presented here show that controlling the short-range interactions between a mixture of suspended species and the solid obstacles in microfluidic devices is a promising strategy to obtain vector separation. To fully characterize the potential of such systems for particle separation, however, further work is needed to investigate the effect that the observed touching collisions have on the hydrodynamic dispersion of finite-size particles in periodic arrays. In addition, we have not considered here possible deviations in the observed dynamical behaviour originated in small perturbations to the system, such as spatial deviations from the periodic structure of the array, fluctuations in the driving force, Brownian motion of the particles and particle-size variations within a given species. Although such effects can significantly affect mechanical dispersion (Koch *et al.* 1989), they are not expected to significantly alter the dynamical behaviour of individual trajectories, other than possibly smoothing the transition between locked states (Heller & Bruus 2008). We observe this behaviour in undergoing macroscopic experiments.

We wish to thank J. F. Brady for making the SD code available to us. We also thank A. Acrivos for his helpful comments on the manuscript. We would like to acknowledge A. Acrivos, J. Koplik and J. F. Morris for useful discussions. G. D. thanks G. Silva and A. Strachan for fruitful discussions and suggestions. This material is partially based upon work supported by the National Science Foundation under grant no. CBET-0731032. Acknowledgment is made to the Donors of the American Chemical Society Petroleum Research Fund for partial support of this research.

REFERENCES

Adamczyk, Z., Adamczyk, M. & Vandeven, T. G. M. 1983 Resistance coefficient of a solid sphere approaching plane and curved boundaries. *J. Colloid Interface Sci.* **96** (1), 204–213.

Allen, M. P. & Tildesley, D. J. 1989 *Computer Simulation of Liquids*. Oxford University Press.

Arnold, V. I 1988 *Geometrical Methods in the Theory of Ordinary Differential Equations*, 2nd ed. Springer.

Austin, R. H., Darnton, N., Huang, R., Sturm, J., Bakajin, O. & Duke, T. 2002 Ratchets: the problems with boundary conditions in insulating fluids. *Appl. Phys.* A **75** (2), 279–284.

Bak, P. 1986 The devil's staircase. *Phys. Today* **39** (12), 38–45.

Bear, J. 1988 *Dynamics of Fluids in Porous Media*. Dover.

Blom, M. T., Chmela, E., Oosterbroek, R. E., Tijssen, R. & van den Berg, A. 2003 On-chip hydrodynamic chromatography separation and detection of nanoparticles and biomolecules. *Anal. Chem.* **75** (24), 6761–6768.

Brady, J. F. & Bossis, G. 1988 Stokesian dynamics. *Annu. Rev. Fluid Mech.* **20**, 111–157.

Brenner, H. 1980 Dispersion resulting from flow through spatially periodic porous-media. *Philos. Trans. R. Soc. Lond.* A **297** (1430), 81–133.

Brenner, H. & Adler, P. M. 1982 Dispersion resulting from flow through spatially periodic porous-media. Part 2. Surface and intraparticle transport. *Philos. Trans. R. Soc. Lond.* A **307** (1498), 149–200.

Brenner, H. & Edwards, D. A. 1993 *Macrotransport Processes*. Butterworth-Heinemann.

Cabodi, M., Chen, Y. F., Turner, S. W. P., Craighead, H. G. & Austin, R. H. 2002 Continuous separation of biomolecules by the laterally asymmetric diffusion array with out-of-plane sample injection. *Electrophoresis* **23** (20), 3496–3503.

daCunha, F. R. & Hinch, E. J. 1996 Shear-induced dispersion in a dilute suspension of rough spheres. *J. Fluid Mech.* **309**, 211–223.

Davis, J. A., Inglis, D. W., Morton, K. J., Lawrence, D. A., Huang, L. R., Chou, S. Y., Sturm, J. C. & Austin, R. H. 2006 Deterministic hydrodynamics: taking blood apart. *Proc. Natl. Acad. Sci.* **103** (40), 14779–14784.

Davis, R. H. 1992 Effects of surface-roughness on a sphere sedimenting through a dilute suspension of neutrally buoyant spheres. *Phys. Fluids* **4** (12), 2607–2619.

Davis, R. H., Zhao, Y., Galvin, K. P. & Wilson, H. J. 2003 Solid–solid contacts due to surface roughness and their effects on suspension behaviour. *Philos. Trans. R. Soc. Lond.* A **361** (1806), 871–894.

Dittrich, P. S., Tachikawa, K. & Manz, A. 2006 Micro total analysis systems: latest advancements and trends. *Anal. Chem.* **78** (12), 3887–3907.

Dorfman, K. D. & Brenner, H. 2001 'Vector chromatography': modeling micropatterned separation devices. *J. Colloid Interface Sci.* **238** (2), 390–413.

Dorfman, K. D. & Brenner, H. 2002 Separation mechanisms underlying vector chromatography in microlithographic arrays. *Phys. Rev.* E **65** (5), 052103.

Drazer, G., Khusid, B., Koplik, J. & Acrivos, A. 2005*a* Hysteresis, force oscillations, and nonequilibrium effects in the adhesion of spherical nanoparticles to atomically smooth surfaces. *Phys. Rev. Lett.* **95** (1), 016102.

Drazer, G., Khusid, B., Koplik, J. & Acrivos, A. 2005*b* Wetting and particle adsorption in nanoflows. *Phys. Fluids* **17** (1), 017102.

Drazer, G., Koplik, J., Acrivos, A. & Khusid, B. 2002*a* Adsorption phenomena in the transport of a colloidal particle through a nanochannel containing a partially wetting fluid. *Phys. Rev. Lett.* **89** (24), 244501.

Drazer, G., Koplik, J., Khusid, B. & Acrivos, A. 2002*b* Deterministic and stochastic behaviour of non-Brownian spheres in sheared suspensions. *J. Fluid Mech.* **460**, 307–335.

Drazer, G., Koplik, J., Khusid, B. & Acrivos, A. 2004 Microstructure and velocity fluctuations in sheared suspensions. *J. Fluid Mech.* **511**, 237–263.

Duke, T. 1998 Separation techniques. *Curr. Opin. Chem. Biol.* **2** (5), 592–596.

Duke, T. A. J. & Austin, R. H. 1998 Microfabricated sieve for the continuous sorting of macromolecules. *Phys. Rev. Lett.* **80** (7), 1552–1555.

Durlofsky, L., Brady, J. F. & Bossis, G. 1987 Dynamic simulation of hydrodynamically interacting particles. *J. Fluid Mech.* **180**, 21–49.

Edwards, D. A., Shapiro, M., Brenner, H. & Shapira, M. 1991 Dispersion of inert solutes in spatially periodic, 2-dimensional model porous-media. *Transport Porous Med.* **6** (4), 337–358.

Eijkel, J. C. T. & van den Berg, A. 2006 The promise of nanotechnology for separation devices: from a top-down approach to nature-inspired separation devices. *Electrophoresis* **27** (3), 677–685.

Ekiel-Jezewska, M. L., Feuillebois, F., Lecoq, N., Masmoudi, K., Anthore, R., Bostel, F. & Wajnryb, E. 1999 Hydrodynamic interactions between two spheres at contact. *Phys. Rev.* E **59** (3), 3182–3191.

Ekiel-Jezewska, M. L., Lecoq, N., Anthore, R., Bostel, F. & Feuillebois, F. 2002 Rotation due to hydrodynamic interactions between two spheres in contact. *Phys. Rev.* E **66** (5), 051504.

Ertas, D. 1998 Lateral separation of macromolecules and polyelectrolytes in microlithographic arrays. *Phys. Rev. Lett.* **80** (7), 1548–1551.

Fannjiang, A. & Papanicolaou, G. 1994 Convection enhanced diffusion for periodic flows. *SIAM J. Appl. Math.* **54** (2), 333–408.

Gadala-Maria, F. & Acrivos, A. 1980 Shear-induced structure in a concentrated suspension of solid spheres. *J. Rheol.* **24** (6), 799–814.

Giddings, J. C. 1991 *Unified Separation Science*. Wiley Interscience.

Goldstein, H. 1980 *Classical Mechanics*, 2nd ed. Addison-Wesley.

Gopinathan, A. & Grier, D. G. 2004 Statistically locked-in transport through periodic potential landscapes. *Phys. Rev. Lett.* **92** (13), 130602.

Grier, D. G. 2003 A revolution in optical manipulation. *Nature* **424** (6950), 810–816.

Hasimoto, H. 1959 On the periodic fundamental solutions of the Stokes equations and their application to viscous flow past a cubic array of spheres. *J. Fluid Mech.* **5** (2), 317–328.

Heller, M. & Bruus, H. 2008 A theoretical analysis of the resolution due to diffusion and size dispersion of particles in deterministic lateral displacement devices. *J. Micromech. Microengng* **18** (7), 075030.

Huang, L. R., Cox, E. C., Austin, R. H. & Sturm, J. C. 2004 Continuous particle separation through deterministic lateral displacement. *Science* **304** (5673), 987–990.

Huang, L. R., Silberzan, P., Tegenfeldt, J. O., Cox, E. C., Sturm, J. C., Austin, R. H. & Craighead, H. 2002 Role of molecular size in ratchet fractionation. *Phys. Rev. Lett.* **89** (17), 178301.

Inglis, D. W., Davis, J. A., Austin, R. H. & Sturm, J. C. 2006 Critical particle size for fractionation by deterministic lateral displacement. *Lab Chip* **6** (5), 655–658.

Jeffrey, D. J. & Onishi, Y. 1984 Calculation of the resistance and mobility functions for two unequal rigid spheres in low-Reynolds-number flow. *J. Fluid Mech.* **139**, 261–290.

Keller, C., Marquardt, F. & Bruder, C. 2002 Separation quality of a geometric ratchet. *Phys. Rev.* E **65** (4), 041927.

Khandurina, J. & Guttman, A. 2003 Microscale separation and analysis. *Curr. Opin. Chem. Biol.* **7** (5), 595–602.

Koch, D. L., Cox, R. G., Brenner, H. & Brady, J. F. 1989 The effect of order on dispersion in porous media. *J. Fluid Mech.* **200**, 173–188.

Korda, P. T., Taylor, M. B. & Grier, D. G. 2002 Kinetically locked-in colloidal transport in an array of optical tweezers. *Phys. Rev. Lett.* **89** (12), 128301.

Lacasta, A. M., Khoury, M., Sancho, J. M. & Lindenberg, K. 2006 Sorting of mesoscopic particles driven through periodic potential landscapes. *Mod. Phys. Lett.* **20** (23), 1427–1442.

Li, Z. & Drazer, G. 2007 Separation of suspended particles by arrays of obstacles in microfluidic devices. *Phys. Rev. Lett.* **98** (5), 050602.

Lin, Y. W., Huang, M. F. & Chang, H. T. 2005 Nanomaterials and chip-based nanostructures for capillary electrophoretic separations of dna. *Electrophoresis* **26**, 320–330.

Malysa, K., Dabros, T. & Van de Ven, T. G. M. 1986 The sedimentation of one sphere past a second attached to a wall. *J. Fluid Mech.* **162**, 157–170.

Marconi, V. I., Candia, S., Balenzuela, P., Pastoriza, H., Dominguez, D. & Martinoli, P. 2000 Orientational pinning and transverse voltage: Simulations and experiments in square Josephson junction arrays. *Phys. Rev.* B **62** (6), 4096–4104.

Masliyah, J. H. & Bhattacharjee, S. 2006 *Electrokinetic and Colloid Transport Phenomena*. Wiley Interscience.

Morris, J. F. & Brady, J. F. 1998 Pressure-driven flow of a suspension: Buoyancy effects. *Intl J. Multiphase Flow* **24** (1), 105–130.

Nitsche, J. M. & Brenner, H. 1988 Sedimentation and dispersion of Brownian particles in spatially periodic potential fields. *J. Chem. Phys.* **89** (12), 7510–7520.

Pamme, N. 2007 Continuous flow separations in microfluidic devices. *Lab Chip* **7**, 1644–1659.

Phillips, R. J., Deen, W. M. & Brady, J. F. 1989 Hindered transport of spherical macro-molecules in fibrous membranes and gels. *AIChE J.* **35** (11), 1761–1769.

Phillips, R. J., Deen, W. M. & Brady, J. F. 1990 Hindered transport in fibrous membranes and gels: Effect of solute size and fiber configuration. *J. Colloid Interface Sci.* **139** (2), 363–373.

Rampall, I., Smart, J. R. & Leighton, D. T. 1997 The influence of surface roughness on the particle-pair distribution function of dilute suspensions of non-colloidal spheres in simple shear flow. *J. Fluid Mech.* **339**, 1–24.

Reichhardt, C. & Reichhardt, C. J. O. 2004 Directional locking effects and dynamics for particles driven through a colloidal lattice. *Phys. Rev.* E **69** (4), 041405.

Reimann, P. 2002 Brownian motors: noisy transport far from equilibrium. *Phys. Rep.* **361** (2-4), 57–265.

Risken, H. 1989 *The Fokker–Planck Equation, Methods of Solution and Application*, 2nd ed. Springer.

Slater, G. W., Desrulsseaux, C., Hubert, S. J., Mercier, J. F., Labrie, J., Boileau, J., Tessier, F. & Pepin, M. P. 2000 Theory of DNA electrophoresis: a look at some current challenges. *Electrophoresis* **21** (18), 3873–3887.

Smart, J. R. & Leighton, D. T. 1989 Measurement of the hydrodynamic surface-roughness of noncolloidal spheres. *Phys. Fluids* **1** (1), 52–60.

Squires, T. M. & Quake, S. R. 2005 Microfluidics: fluid physics at the nanoliter scale. *Rev. Mod. Phys.* **77** (3), 977–1026.

Szantai, E. & Guttman, A. 2006 Genotyping with microfluidic devices. *Electrophoresis* **27** (24), 4896–4903.

Szekely, L. & Guttman, A. 2005 New advances in microchip fabrication for electrochromatography. *Electrophoresis* **26** (24), 4590–4604.

Tegenfeldt, J. O., Prinz, C., Cao, H., Huang, R. L., Austin, R. H., Chou, S. Y., Cox, E. C. & Sturm, J. C. 2004 Micro- and nanofluidics for DNA analysis. *Anal. Bioanal. Chem.* **378** (7), 1678–1692.

Vilkner, T., Janasek, D. & Manz, A. 2004 Micro total analysis systems: recent developments. *Anal. Chem.* **76** (12), 3373–3385.

Weinan, E. 1992 Homogenization of linear and nonlinear transport-equations. *Comm. Pure Appl. Math.* **45** (3), 301–326.

Zeng, S. L., Kerns, E. T. & Davis, R. H. 1996 The nature of particle contacts in sedimentation. *Phys. Fluids* **8** (6), 1389–1396.

Zhao, Y. & Davis, R. H. 2002 Interaction of two touching spheres in a viscous fluid. *Chem. Engng Sci* **57** (11), 1997–2006.

Zhao, Y. & Davis, R. H. 2003 Interaction of sedimenting spheres with multiple surface roughness scales. *J. Fluid Mech.* **492**, 101–129.